Fabrication and customization of highly porous PLGA membranes utilizing near-field electrospinning, thermal transitions, and multilayer strategies

Noori Na, Minju Kim, Jungkyu Kim*, and Jiyoung Chang*

Department of Mechanical Engineering, University of Utah, Salt Lake City, USA

Corresponding author: jy.chang@utah.edu, jkim@mech.utah.edu

Abstract

Polymer porous membranes play a crucial role in various applications, including water filtration, tissue engineering, and drug administration. Conventional electrospinning is employed for the production of polymeric membranes because of its cost-effectiveness, scalability, and the flexibility. However, it has limitations in terms of controlling the form and size of the pores. Ensuring the ability to maintain a consistent and customizable pore size without sacrificing the thickness of the membrane becomes more crucial to satisfy the various requirements of cell and tissue engineering applications. To address these limitations, this work combines Near-Field Electrospinning with thermal treatment of polymer fibers and membranes by exploring the connection between polymer behavior, thermal effects, and capillary action by measuring the fluctuations in pore area under different temperatures and fiber spacings. Furthermore, the study investigated the influence of multilayer infusion on pore size and geometric arrangement by investigating multiple-layer configurations stacked at different angles. The results indicated that increasing layers leads to decreasing pore size, while the alignment of infused fibers adds to differences in pore form. By enabling enhanced control over membrane characteristics, the proposed approach can enhance the performance and consistency of polymer porous membranes in a wide range of applications.

Keywords: Porous membrane, polymeric fiber, near-field electrospinning, thermal infusion, organ chip

1. Introduction

Polymer porous membranes are widely used for their diverse applications, spanning water filtration [1-3], tissue engineering [4, 5], and drug delivery[6-8] due to their flexibility, biocompatibility, cost-effectiveness, and tunable mechanical characteristics. Specifically, creating controllable and uniform membrane pore sizes is the main focus for manufacturing membranes for multiple applications. For example, uniform pore sizes are crucial for ensuring consistent and predictable filtration performance in membrane-based separation processes. Irregular pore sizes can lead to uneven flow rates and reduced filtration efficiency, negatively impacting the membrane performance to separate particles based on size with high selectivity [9-11]. In drug delivery systems, uniform pore sizes play a crucial role in achieving precise control over the release rate of therapeutic agents, particularly in controlled-release formulations. The uniform pore structure of the membrane is essential for regulating drug release accurately and consistently. By maintaining well-defined pore size and distribution, the membrane can ensure a predictable and controlled release profile, enhancing the treatment's effectiveness. Uniform pores allow for steady and reproducible diffusion of the drug molecules through the membrane, minimizing variations in release kinetics and improving the overall performance of the drug delivery system. [12-15]. Furthermore, polymeric porous membranes are commonly used in tissue engineering, where scaffolds support cell growth and tissue regeneration [16-19]. Different cells exhibit distinct preferences for pore size; smaller pores facilitate cell migration and proliferation, while larger pores facilitate cell attachment and growth. This preference has been evidenced by studies examining the impact of pore size on cell adhesion, proliferation, growth, and cell-cell communications [20-22]. This difference in cell behavior arises from the limited space available for cell attachment in smaller pores. In contrast, larger pores facilitate enhanced diffusion of nutrients and oxygen, thereby supporting cell growth and metabolic activities [23].

Polymeric porous membranes are commonly fabricated using techniques such as track etching, lithography, and soft lithography [24-26]. However, electrospinning has emerged as a major membrane manufacturing process due to its scalability, straightforward process, and ability to produce membranes with a high surface-to-volume ratio. Despite these advantages, traditional far-field electrospinning encounters significant challenges in creating ordered patterns [27, 28] due to the extended distance between the spinneret and the collector, coupled with the erratic trajectory of the ejected jet, leading to a random deposition of fibers. Consequently, the porosity of the membranes is intrinsically dependent on the size of individual pores; thus, controlling the porosity becomes a complex task, as it requires altering the membrane thickness, introducing additional complexities to the fabrication process. To address the challenges associated with far-field electrospinning, Wang et al. conducted a study investigating the impact of solution concentration on fiber formation [29] in which they explored how varying solution concentrations influenced the formation of fibers and the resulting morphology. By establishing relationships between fiber diameter, membrane thickness, pore size, and pore size distribution, filtration efficiency was optimized for separating micro-particles and bacteria.

Although far-field electrospinning techniques are useful for membrane fabrication, precisely controlling the pore size and porosity using the far-field electrospinning process remains a major challenge. To address this limitation, the near-field electrospinning (NFES) technique has emerged as a promising approach, offering enhanced control over fiber deposition onto the substrate. By significantly reducing the distance between the spinneret and collector, NFES allows for patterning of fibers rather than random deposition [30-32]. Numerous studies have demonstrated the ability of NFES to fabricate patterned bio-scaffolds and membranes for applications such as tissue engineering [33, 34], drug delivery [35, 36], and biosensing [37, 38]. However, the control over polymer pore size and porosity in NFES primarily relies on fiber spacing and initial fiber diameter, which can be challenging to precisely control, especially in the micrometer or smaller range. This challenge often necessitates re-fabricating membranes or scaffolds to achieve varying pore sizes.

An alternative strategy to modulate the pore size and porosity of electrospun polymer membranes is through post-fabrication thermal annealing. Typically, polymers exhibit relatively low glass transition temperatures. When subjected to thermal treatment above their glass transition temperature, the polymer structure can be reconstructed, allowing individual fibers to spread and merge at fiber junctions. This process presents an opportunity to tailor the membrane properties and pore shape and size. For instance, a poly(glycolic acid) (PGA) fiber-based scaffold was fabricated using the far-field electrospinning technique, and the scaffold was subsequently immersed in a poly(L-lactic acid) (PLLA)/methylene chloride solution [39]. After evaporating the solvent, the polymer composite was heated above the melting point of PLLA. This process selectively dissolved the PLLA, allowing it to act as a glue between the PGA fibers at their cross-points, ultimately strengthening the scaffold structure. In addition to the selective scaffold manufacturing process, thermal annealing processes were used to enhance mechanical properties and control the pore size of poly(lactic acid) (PLA) electrospun membranes [40]. The annealed membrane exhibited an 8-fold difference compared to the untreated membrane, indicating a significant enhancement in mechanical stiffness through thermal treatment. Additionally, variations in annealing time and temperature resulted in reductions in pore size. However, despite these improvements, controlling individual pore sizes remains challenging in far-field electrospun membranes. The effects of thermal treatment on electrospun polystyrene (PS) and poly(methyl methacrylate) (PMMA) fibers were also examined to investigate the internal porosity and mechanical properties of the fibers by controlling cooling rates and annealing conditions [41, 42]. These studies show that higher annealing temperatures, longer annealing times, and slower cooling rates were needed to induce the desired mechanical deformation and transformation of the electrospun polymer fibers. Although these studies have investigated the effects of different annealing conditions on polymer morphology and pore structure, these studies have primarily focused on far-field electrospun fibers. Consequently, a comprehensive understanding of the spreading behavior of individual fibers and pore size control is still lacking.

In this study, we aim to address the trade-off between achieving smaller pore sizes and increased deposition time, which can lead to undesired membrane thickness, by introducing a

synergistic approach combining near-field electrospinning (NFES) and controlled phase change of polymers through thermal annealing above the glass transition temperature (Figure 1). Specifically, we investigate the interplay between fiber manufacturing parameters, temperature-induced transitions, and multilayer infusion, enabling precise control over pore sizes in poly (lactic-co-glycolic acid) (PLGA) membranes. Notably, accurate control of the annealing temperature and duration is crucial in governing the spreading behavior of individual electrospun fibers and the merging of fibers at fiber junctions, thereby enabling the formation of membranes with tailored pore sizes and porosities. The insights derived from this work are expected to provide valuable guidance for future membrane fabrication processes, facilitating the production of membranes with tailored and consistent porosity for various applications.

2. Materials and Methods

Poly(D, L-lactide-co-glycolide) (PLGA), a synthetic copolymer derived from polylactic acid (PLA) and polyglycolic acid (PGA), has garnered significant attention as a preferred material for scaffold construction [43-45]. This popularity is attributed to its favorable characteristics, including the ability to tailor degradation rates, exceptional mechanical strength and toughness, and straightforward processing [46]. Moreover, PLGA exhibits the advantage of being easily electrospun into fiber form [47, 48]. In the current study, a PLGA solution with a concentration of 13 wt% was selected after a thorough comparison with other weight percentages, demonstrating superior uniformity in the solution. This concentration was deemed optimal for subsequent fabrication processes.

2.1 Nearfield Electrospinning (NFES)

Poly(D, L-lactide-co-glycolide) (PLGA 75:25) with a molecular weight ranging from 66,000 to 107,000 and 1,1,1,3,3,3-Hexafluoro-2-propanol (HFP) were procured from Sigma-Aldrich. PLGA pellets, constituting 13 wt% of the solution, were introduced into HFP and thoroughly mixed for 24 hours at room temperature. PLGA membranes were fabricated using a Nearfield Electrospinning (NFES) system, comprising an XYZ controllable stage (ONE-XY100 for XY axis, one μm resolution, GTS30 V for Z-axis, 0.1 μm resolution, Newport), a long-distance microscope (K2 Distamax, Infiniti, Basler ace), a voltage supply (PS350, Standford Research System), a USB camera (Koolertron), and a pneumatic pump (Ultimus V dispenser, Nordson). These components were meticulously coordinated through a LABVIEW (National Instruments) graphical user interface (GUI) program. A PLGA polymer solution was injected into a 3cc syringe with a 30-gauge needle to achieve the desired fiber diameter. The top part of the syringe was connected to the pneumatic pump with an airflow to maintain a droplet on the tip. To investigate the impact of these parameters on fiber diameter and, consequently, pore size, a comprehensive exploration was conducted following the parameters outlined in Table 1. Various experimental factors were examined to assess the impact on fiber diameter, including collector speed (6, 8, 10 mm/s), applied voltage (600, 700, 800, 900, 1000V), and tip-to-collector distance (0.1, 0.2, 0.3 mm). The pressure was minimized to facilitate droplet formation at the needle tip, while the solution concentration

remained fixed at 13 wt%, chosen for its superior solution uniformity. Fiber diameter assessment involved measuring the average diameter of 10 fibers for each parameter, excluding any irregular fibers. Conditions of 600V, a collector speed of 10mm/s, and a tip-to-collector distance of 0.1mm were selected based on the uniformity and the suitability for membrane applications, with the average fiber diameter ranging from 7 - 10 μm.

Table 1. NFES Parameters

Parameter	**Values**
Applied Voltage	600 – 1000 V increased by 100V
TTCD	0.1 – 0.3 mm increased by 0.1 mm
Collector Speed	6 – 10 mm/s increased by 2 mm/s

2.2 Observation of Temperature Impact on PLGA Fiber Morphology and Membrane Pore Area

Upon subjecting fibers to a 1-hour heat treatment at diverse temperatures and subsequent scanning electron microscope (SEM) examination, the height and diameter ratio of the fibers were determined by averaging measurements from approximately ten fibers for each temperature, as outlined in Figure 3 (d). Following optimal parameters for PLGA fiber production, membranes were fabricated with diverse spacings (50, 70, and 100 μm) along the XY axis to explore the influence of temperature on pore area. Utilizing a microscope (model M Plan Apo5, Mitutoyo) with a CCD camera (model MU1403, AmScope), pore areas of the grid-shaped membranes were observed. Subsequently, the membranes underwent a one-hour heating process at varying temperatures and spacings on a hotplate, with temperature validation conducted using an infrared thermometer. Images of the same membrane region were systematically captured at 15-minute intervals to monitor alterations in pore areas over time comprehensively. This observation and fabrication process allowed for a detailed examination of how temperature affects the morphology and pore size of PLGA membranes.

2.3 Measurement using Scanning Electron Microscope (SEM)

To examine the cross-section of fibers after one hour of heat treatment at different temperatures, the SEM (FEI Quanta 600 FE-ESEM) technique was employed. Ten PLGA fibers were deposited on four individual silicon wafers. One sample was maintained at room temperature, while the other three samples were heated at 50°C, 70°C, and 90°C, followed by immersion in liquid nitrogen and subsequent fracturing to observe fiber cross-sections. Before measurements, the samples were coated with an approximately 10 nm layer of platinum-gold to prevent charging effects during SEM operation.

2.4 Observation of Multilayer Membrane

In this experimental setup, two, four, six, and eight-layer configurations of membranes were superimposed at distinct angular orientations (~45° for the four-layer configuration ~30° and ~60° for the six-layer configuration, and ~20° each for eight-layer configuration, Figure 5). The

multilayer membrane was observed using a CCD camera (MU1403, AmScope) and AmScope software in conjunction with a microscope (M Plan Apo 5, Mitutoyo). The objective was to illustrate variations in pore shapes and sizes resulting from the specific overlapping angles. Following each layer's precise alignment and superimposition, the composite membranes were subjected to heat treatment on a hotplate for an hour. This thermal treatment aimed to induce the merging of individual layers, consolidating them into a singular, integrated layer. The pore size distribution for each configuration was determined using Image J software. A total of ten photographs were captured randomly from three distinct membrane samples for each configuration, and subsequent analysis was performed to ascertain the distribution of pore sizes.

2.5 Cell culture on the membrane

To investigate cell viability and cell attached pattern on the six-layered membrane, a PDMS mold was designed to support a suspended membrane as illustrated in Figure 6(a). PDMS (SYLGARD 184, DOW Corning, USA) was utilized with a 10:1 ratio of base and cross-linker agent. After degassing the PDMS mixture in a vacuum chamber for 30 minutes, it was cured overnight at 60 °C in a dry oven, using a 100-mm petri dish, to form a 2-mm thick layer of PDMS. The cured PDMS was cut with a 10-mm diameter puncher as the outer line, and a 6-mm diameter hole was punched for the inner hole. To fix the six-layered membrane on PDMS mold, uncured PDMS mixture was applied as an adhesive by stamping onto the PDMS mold. The membrane was then positioned on the adhesive coated PDMS mold, and the assembly was cured at room temperature overnight. Primary human corneal keratocytes (HCK, ScienCell, USA) were cultured by following the manufactural instruction using Fibroblast Medium (ScienCell, USA) containing 2% fetal bovine serum (FBS, ScienCell, USA), 1% FCS (fibroblast growth supplement, ScienCell, USA), and 1% P/S (antibiotic solution, ScienCell, USA) on a poly-L-lysine (10 mg/ml, ScienCell, USA) coated flask. The fourth passaged HCK was seeded on the membrane with 3×10^6 cells/mL. The culturing cells on the suspended membrane were stained with 10μM Cell Tracker™ Green CMFDA dye (C7025, Thermo Fisher Scientific, USA). Nikon Eclipse Ti fluorescence microscope with the NIS Element software was used to take cell images.

3. Results and Discussion

3.1 Optimization of NFES Parameters for PLGA Fiber Fabrication

To fabricate a porous PLGA membrane with uniform pore sizes, the optimization of nanofiber electrospinning parameters, such as voltage, pressure, tip-to-collector distance (TTCD), and collector speed, which influence the diameter of the resulting fibers, is essential. These parameters were systematically managed through a customized LABVIEW graphical user interface (GUI). **Figure 2(a)** illustrates a brief example of the parameters of the NFES system, where the applied voltage, TTCD, and the collector velocity can be easily adjusted using LABVIEW GUI. **Figures 2 (b-d)** depict the influence of individual parameters on fiber diameter, with the other parameters fixed at 600V applied voltage, 0.1mm TTCD, and 10 mm/s collector speed. **Figure 2(b)** indicates that an increase in collector speed results in a thinner fiber diameter, although beyond 8mm/s, the

fiber diameter exhibits minimal change for all TTCD values. **Figure 2(c)** demonstrates that an increase in applied voltage corresponds to an increase in fiber diameter, regardless of collector speed. **Figure 2(d)** reveals that an increase in TTCD leads to an increase in fiber diameter for all applied voltages. An analysis of variance (ANOVA) test indicated the significance of all three parameters. However, TTCD emerged as the least significant among them. In this study, we thoroughly investigated how factors like applied voltage, TTCD, and collector speed affect the diameter of PLGA fibers produced through NFES. Through systematic adjustment and analysis, the study identifies optimal NFES parameters (600 V applied voltage, 0.1 mm TTCD, and 10 mm/s collector speed) for achieving uniform fiber diameter within the desired range (7 - 10 μm). These parameters were selected based on their demonstrated efficacy in producing fibers with consistent diameters. While TTCD appeared to have the least impact compared to the other parameters, it still played a role in influencing fiber diameter. This optimization is crucial for membrane fabrication, ensuring uniformity in pore size distribution across the membrane. Our findings offer valuable insights for refining NFES techniques in PLGA fiber production, with implications for various biomedical applications requiring precise control over fiber characteristics.

3.2 Analysis of Polymeric Fiber Morphology with Temperature Variation

As polymeric fibers approach or surpass their glass transition temperature, they undergo significant changes in their cross-sectional shape. **Figure 3 (a-c)** illustrates the effect of various temperatures on fiber formation, highlighting the necessity for precise cross-sectional shape prediction to understand these variations accurately. A clear correlation is observed between elevated temperatures and increased fiber diameter, accompanied by a reduction in fiber height. This height reduction occurs due to the polymer transitioning into a rubbery state, characterized by increased molecular mobility and the relaxation of the molecular structure. The rubbery state allows fibers to spread more easily, aided by the enhanced molecular mobility, resulting in a larger cross-sectional diameter. The initial rapid spreading within the first 15 minutes is attributed to the heightened molecular mobility during the transitional period. **Figure S1** presents a Quantitative analysis, showing average fiber diameter changes of approximately 1%, 5%, and 50% after one hour at 50°C, 70°C, and 90°C, respectively. Fiber diameter changes during the annealing process, and the extent of this change depends on three key factors: initial fiber diameter, annealing time, and annealing temperature. Among these factors, temperature plays the most significant role in determining the final fiber diameter. As the annealing process progresses, the spreading of fibers slows down due to the limited volume of material within each fiber. Consequently, as the fiber diameter increases due to the collapse of fiber height, the overall thickness of the electrospun membrane decreases with increasing annealing temperature. These observations are consistent with the findings reported in a previous study. [40]. The substantial impact of heat treatment above the glass transition temperature on the morphological characteristics of PLGA fibers, providing better understanding of the complex relationship between temperature-induced transitions and resulting fiber morphology.

3.3 Analysis of Pore Area Difference with Temperature Variation

As elucidated by prior studies, controlling pore size is a critical aspect of membrane fabrication [9, 10]. As previously discussed, individual fibers exhibit a spreading behavior when exposed to temperatures exceeding the glass transition temperature of PLGA. Conversely, when two layers of fibers are patterned orthogonally, the intersections in the x-y plane form junctions. Heating the membrane facilitates the merging and spreading of junctions, establishing a robust bond and reducing overall membrane thickness [39]. Observing the spreading phenomenon of PLGA along with varying fiber spacing allows the pore size of the membrane to be precisely controlled.

Figure 4 presents the impact of various spacings and temperatures on pore morphology. At 50 °C, minimal changes in pore sizes were observed across all three spacings. At 70 °C, slight diameter spreading was noted, and the junctions between fibers began to fuse, creating a bond. Notably, at 90 °C, significant fiber spreading occurred, with complete fusion of junctions. It was reported that in far-field electrospinning, PLA fibers start merging at their junctions after a 30-minute annealing process at 90°C [40]. However, in the case of PLGA, which combines PGA with PLA and thus has a lower glass transition temperature, the fusion of PLGA fiber junctions occurs notably earlier, within just 15 minutes of annealing at 90°C . It is essential to highlight that smaller spacing correlates with increased changes in pore size area. These phenomena can be explained by considering a combination of factors, including polymer behavior, thermal effects, and capillary action. As PLGA undergoes thermal softening above its glass transition temperature, the fibers become more flexible, facilitating their spreading. Elevated temperatures induce molecular mobility, potentially leading to partial melting and fusion of fibers at junctions. Capillary action, the ability of a liquid to flow in narrow spaces without external force, is also implicated. Smaller spaces between fibers result in higher capillary pressure, further influencing pore size. In essence, the interplay of spacing and temperature provides a mechanism for tuning membrane porosity. Using ImageJ software, an in-depth analysis of pore surface areas was conducted on membranes with varied spacings subjected to temperatures of 50 °C, 70 °C, and 90 °C. **Figure 4(d)** shows the temperature-dependent changes in pore area at 50 μm spacing, while **Figure 4(e)** delineates alterations in pore area at 90 °C for different spacings. The results underscore a noticeable augmentation in pore size, particularly within the initial 15 minutes, aligning with the rapid changes observed in the spreading behavior of individual fibers under elevated temperatures. The quantitative assessment involved computing the percentage change in pore area following a 1-hour exposure. For the 50 μm spacing, the changes were 1.0%, 2.2%, and 29.3% at 50 °C, 70 °C, and 90 °C, respectively, revealing a temperature-dependent trend with higher temperatures inducing more pronounced and accelerated changes in pore size early in the exposure. The observed changes at 90 °C exhibited distinct magnitudes for different spacings, with percentages recorded as 29.3%, 15.2%, and 10.5% for spacings of 50 μm, 70 μm, and 100 μm, respectively (**Figure 4 (e)**. The variations in capillary flow at junctions contribute significantly to these trends. Smaller fiber spacings, such as 50 μm, exhibit enhanced capillary action, leading to more substantial merging and spreading at the junctions, resulting in higher percentage differences in pore area compared to larger spacings, such as 100 μm, where capillary flow is comparatively less pronounced, yielding

lower percentage differences in pore area. This non-linear relationship underscores the intricate interplay between capillary flow and fiber spacing during the thermal treatment. The capillary action at the junctions of the fibers becomes a governing factor in the redistribution of the polymer material, influencing the final morphology of the pores in a spacing-dependent manner. This insight into capillary dynamics contributes to a more comprehensive understanding of the mechanisms dictating the changes in pore area in response to thermal treatment, providing valuable guidance for optimizing membrane fabrication processes.

Manipulating the pore size in PLGA membranes involves a nuanced control of various fabrication parameters. Pore dimension reduction can be achieved through strategic adjustments, such as decreasing inter-fiber spacing or increasing individual fiber diameters. The tuning of manufacturing parameters, encompassing variables such as the poly(lactic acid) (PLA) to poly(glycolic acid) (PGA) ratio, PLGA weight percentage (wt%), and manipulating the parameters during the electrospinning process, contributes to the modulation of membrane morphology. Specifically, a decreased spacing between adjacent fibers influences the overall porosity by restricting the available space for pore formation. Simultaneously, an increase in fiber diameter contributes to a reduction in pore size , owing to the inherently smaller inter-fiber spaces generated by larger fiber dimensions. Furthermore, the anisotropic manipulation of membrane architecture is attainable by employing different spacings along the X and Y axes during fabrication. This deliberate spatial variation results in membranes with directional disparities in pore sizes, offering a versatile approach to tailor membrane properties based on specific application requirements. Beyond parameter adjustments within the PLGA system, the thermal properties of alternative polymers present an avenue for tailoring pore sizes. A diversified range of pore sizes can be achieved by harnessing the distinct thermal characteristics of polymers, such as their glass transition temperatures (Tg) or melting points. This approach extends the scope of membrane design, enabling customization by selecting polymers with thermal attributes aligned with the desired membrane characteristics. In essence, the precise control of manufacturing parameters and the strategic incorporation of alternative polymers with tailored thermal properties delineate a sophisticated framework for engineering PLGA membranes with finely tuned pore sizes. This multifaceted approach provides a comprehensive toolkit for addressing diverse applications in controlled-release systems, tissue engineering, and other domains where precise control over membrane porosity is paramount.

3.4 Multilayer Membrane Infusion

The manipulation of pore size within a fibrous structure can be achieved through various methodologies, such as adjusting the inter-fiber spacing and employing larger-diameter fibers during manufacturing. Additionally, the introduction of multiple layers at different angles offers a versatile means to regulate pore size and influence the overall geometric configuration of the pores. **Figure 5(a)** shows how to implement a four-layer infusion at an elevated temperature of 90°C, resulting in the formation of a distinctive triangular pore morphology. In **Figure 5(b)**, a six-layer infusion conducted under identical temperature conditions manifests a more compact and circular

pore configuration. The delineation of pore areas across distinct infusion layers is meticulously presented in **Figure 5(c)**. Notably, the pore areas associated with more than six-layer infusions predominantly fall below 100 μm², closely resembling a circular shape with an estimated diameter of approximately 10 μm (**Figure S2(b)**). However, an observable trend emerged as more layers were infused into the membrane, the pore area decreased, likely due to the increased density of fibers. Interestingly, as the fibers melted during the process, they contributed to filling up the pore spaces, resulting in a reduction in the overall number of pores (**Figure S2(a)**). In contrast, the triangular morphology observed in four-layer pore areas exhibits a wider area distribution. This distinctive feature can be attributed to the infusion being executed at a 45° angle, resulting in predominantly triangular shapes. However, it is noteworthy that the imperfect infusion at this specific angle contributes to a more extensive distribution of pore areas. This phenomenon is primarily a consequence of the small holes formed during the imperfect infusion process at the 45° angle, which introduces variability in the size and shape of the resulting pores. For two-layer infusions, the distribution of pore areas is centered around 1200-1400 μm², corresponding to an approximate length of 35-37 μm in the context of a square. This observation underscores the nuanced interplay between the infusion angle and inter-fiber spacing, influencing the resultant pore morphology and area distribution.

An alternative approach to the merger of two-layer membranes at various angles involves direct patterning on top of each layer. In this context, the third layer was intricately patterned directly onto the second layer at a 45° angle. While offering a more precise and accurate means of patterning, this method introduces a consideration regarding the impact of increased layering on near-field electrospinning (NFES) characteristics. As layers accumulate, the electric field changes, subsequently influencing the NFES characteristics. This highlights the intricate balance between achieving precision in patterning and acknowledging the evolving electrospinning dynamics with each additional layer, thereby necessitating a nuanced approach in optimizing layering strategies for near-field electrospinning applications. This study demonstrates the effectiveness of the proposed method in modifying pore size and shape. The number of layers and the orientation of infused fibers are identified as the most important factors that influence pore morphology. As the number of layers increases, the pore size decreases. To achieve precise control over pore characteristics, it is essential to implement accurate programming during the manufacturing process. This programming should specify the dimensions and arrangement of fibers to obtain the desired pore shape and size.

3.5 Cell viability test and characteristics on multi-layered membrane

To demonstrate the utilization of the membranes, HCK cells were cultured on both heated and non-heated multilayered membranes. As presented in **Figure 6(b)**, HCK cells seeded on a non-heated membrane showed a lower cell density than those on the heated membrane due to bigger pore size. The cells attached to the non-heated fibers exhibited shallow and spindle shapes, aligning closely with the orientation of PLGA fibers. Furthermore, the cells preferred attaching to denser fiber areas over more sparse ones within the same membrane. In contrast, the heated membrane showed

around 2.5 times higher cell density than the non-heated membrane due to its smaller pore sizes, despite the same initial seeding conditions. Furthermore, the cells on the heated membrane showed around 1.4 times wider cell morphology with stable attachment compared to the non-heated membrane. These findings suggest that the non-heated membranes offer advantages in studying cell alignment and orientation in response to the orientation of PLGA fibers. On the other hand, the non-heated membrane reduces cell loss by decreasing the pore size and enhances cell adhesion by providing a larger surface area, thereby creating more supportive environments for cell culture without any trade-off in cell proliferation rate as observed in **Figures 6(b) and 6(c)**. From the cell culture demonstration, the multilayered PLGA membranes with both heat and non-heat treatment can serve as biocompatible environments to support cell culture, potentially useful for tissue engineering research.

4. Conclusion

To summarize, the NFES method was effectively utilized to produce PLGA membranes with consistent and adjustable pore diameters that are not influenced by the thickness of the membrane. The thermal annealing of the PLGA membrane, in conjunction with the fiber spacing control method, has been proven to be an efficient technique for altering the shape of electrospun fibers. This alteration occurs when the fibers are heated over their glass transition temperature. An examination of the changes in the shape and structure of polymeric fibers at different temperatures showed that the size of the pores may be controlled by adjusting the temperature. Higher temperatures caused considerable changes in pore size, especially during the first 15 minutes. The use of a multi-layered membrane technique led to the creation of a fused membrane that has a smaller pore size but a lower pore density. The number of layers has a direct correlation with reducing pore size and density, providing an additional method to regulate both pore size and density in a membrane with a starting pore size. Further investigation is warranted to study the impact of multilayer infusion methods on the characteristics of membranes, including their permeability and mechanical strength which are are essential for enhancing the design and performance of these membranes in many biomedical applications.

Figures

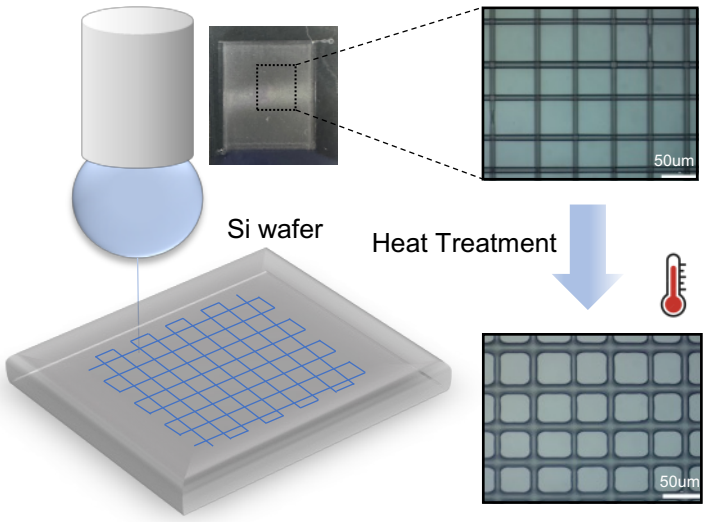

Figure 1. Tunable porous membrane fabricated by near-field electrospinning (NFES) and subsequent heat treatment.

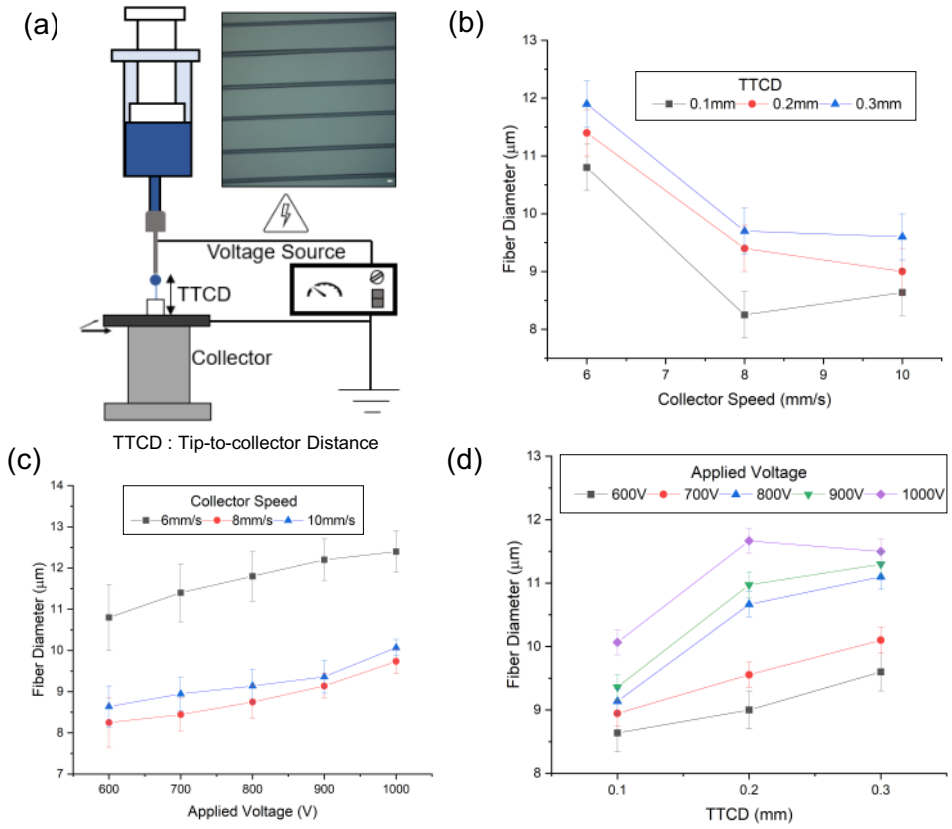

Figure 2. Fiber diameter control by adjusting voltage, TTCD (tip-to-collector distance), and collector speed. (a) Schematic of Electrospinning System (b) Applied Voltage 600V (c) TTCD 0.1mm (d) Collector speed 10mm/s.

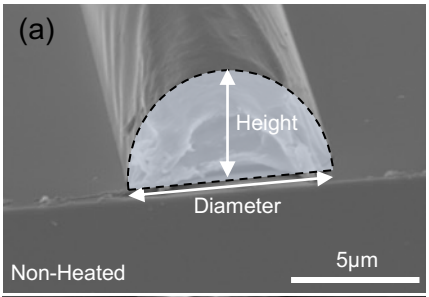

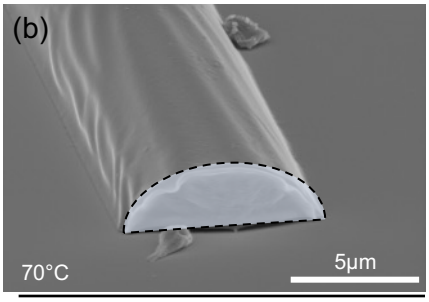

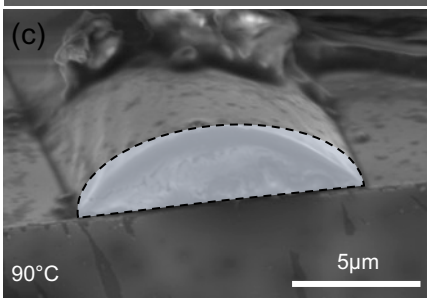

(d)

Temperature	Height / Diameter Ratio
Non-Heated	0.46
50°C	0.45
70°C	0.37
90°C	0.25

Figure 3. SEM images showing the change in fiber height and diameter at different temperatures. (a) Non-heated fiber, (b) 70°C, (c) 90°C, (d) Height/Diameter ratio at different temperatures.

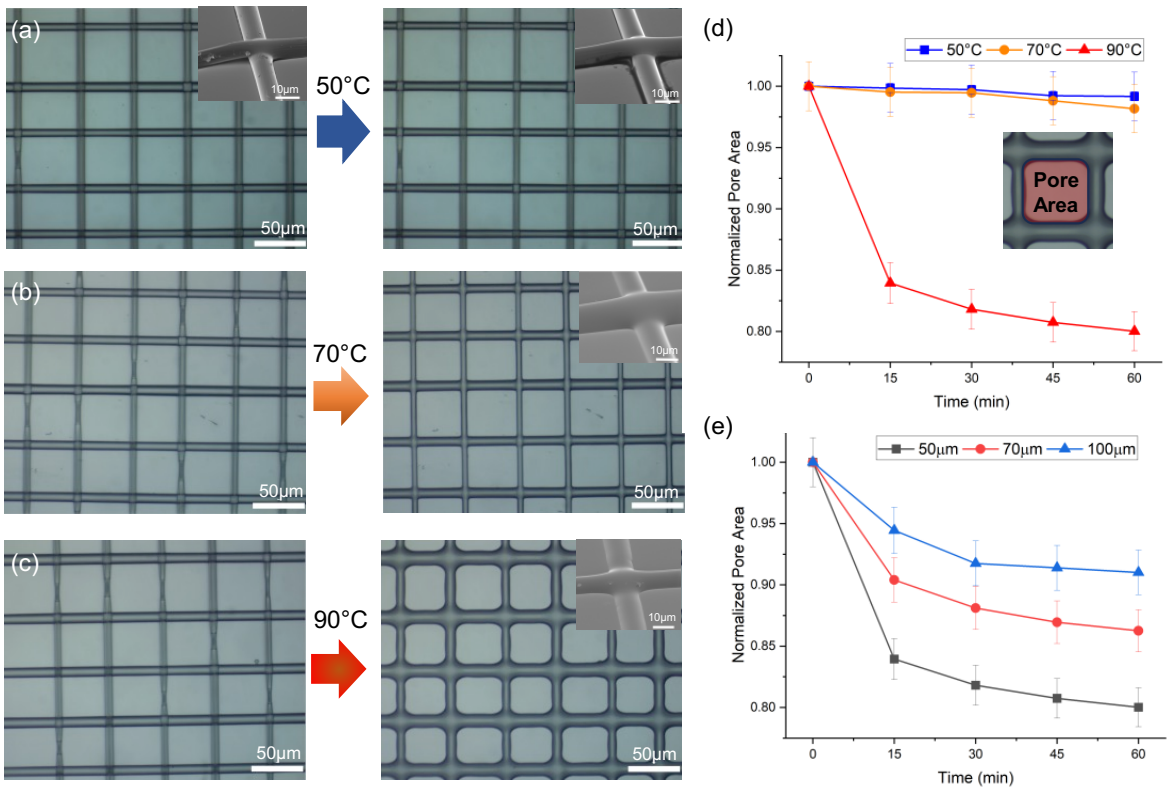

Figure 4. Morphology of pores and fiber junctions in electrospun membranes subjected to different heat treatment temperatures at a constant fiber spacing of 50 µm: (a) 50°C, (b) 70°C, (c) 90°C. (d) Variation in pore area with heat treatment temperature at 50 µm fiber spacing. (e) Pore area change at 90°C for different fiber spacings.

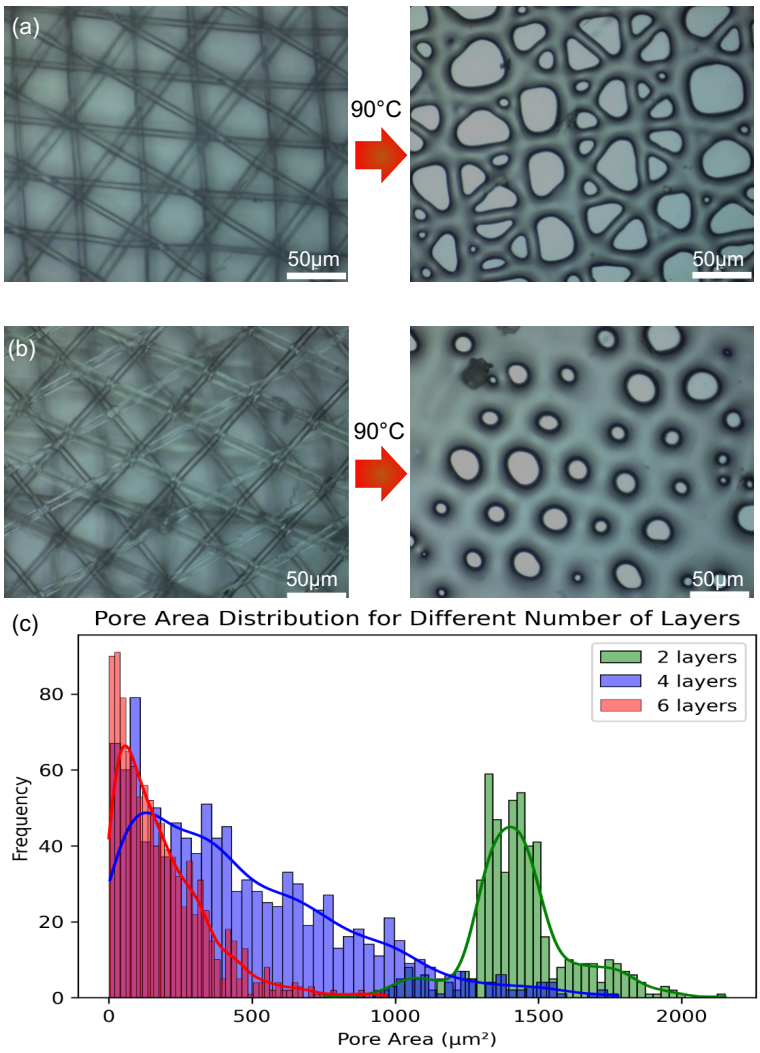

Figure 5. Pore size tuning in multilayered electrospun membranes by heat treatment. (a, b) Microscope images of 4- and 6-layer membranes before and after heating at 90°C for 1 hour. (c) Pore size distributions for different layer counts, demonstrating pore size modulation.

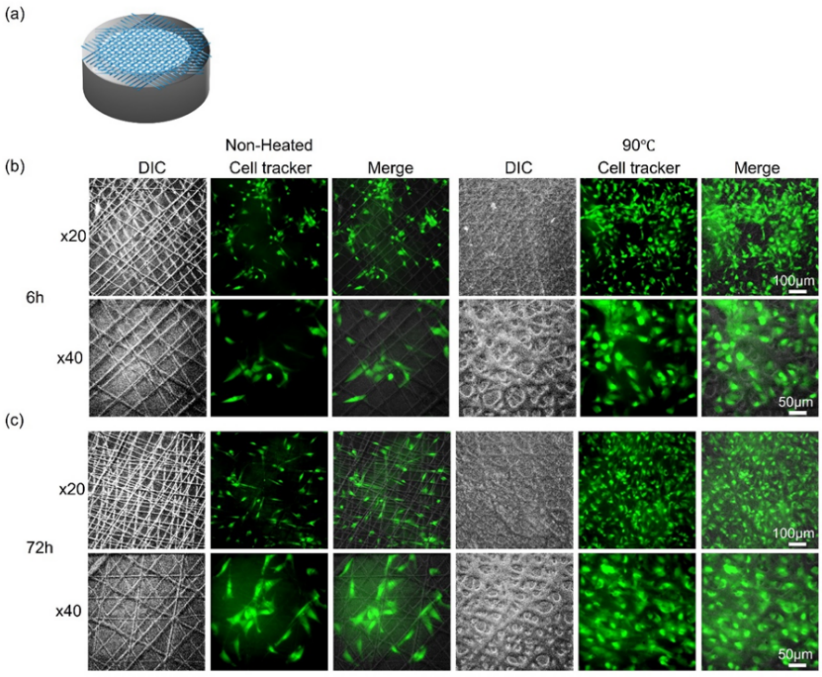

Figure 6. Comparison of culturing cells on the non-heated and heated (90°C) membranes. (a) Illustration of a PDMS mold supporting a six-layered membrane. (b) CellTracker^{TM} CMFDA stained HCK cell images captured with 20x and40x magnification, 6 hours after initial seeding. (c) Cell images after 72 hours.

References

1. Geise, G.M., et al., *Water purification by membranes: the role of polymer science.* Journal of Polymer Science Part B: Polymer Physics, 2010. **48**(15): p. 1685-1718.
2. Kaiser, A., W.J. Stark, and R.N. Grass, *Rapid production of a porous cellulose acetate membrane for water filtration using readily available chemicals.* Journal of chemical education, 2017. **94**(4): p. 483-487.
3. Xie, W., et al., *An aquaporin-based vesicle-embedded polymeric membrane for low energy water filtration.* Journal of Materials Chemistry A, 2013. **1**(26): p. 7592-7600.
4. Das, P., et al., *Development of double porous poly (ε-caprolactone)/chitosan polymer as tissue engineering scaffold.* Materials Science and Engineering: C, 2020. **107**: p. 110257.
5. Nunes-Pereira, J., et al., *Poly (vinylidene fluoride) and copolymers as porous membranes for tissue engineering applications.* Polymer Testing, 2015. **44**: p. 234-241.
6. Arruebo, M., *Drug delivery from structured porous inorganic materials.* Wiley Interdisciplinary Reviews: Nanomedicine and Nanobiotechnology, 2012. **4**(1): p. 16-30.
7. McHugh, A., *The role of polymer membrane formation in sustained release drug delivery systems.* Journal of controlled release, 2005. **109**(1-3): p. 211-221.
8. Sellergren, B. and C.J. Allender, *Molecularly imprinted polymers: A bridge to advanced drug delivery.* Advanced drug delivery reviews, 2005. **57**(12): p. 1733-1741.
9. Antony, A., J. Blackbeard, and G. Leslie, *Removal efficiency and integrity monitoring techniques for virus removal by membrane processes.* Critical Reviews in Environmental Science and Technology, 2012. **42**(9): p. 891-933.
10. Deng, Y., et al., *Bio-based electrospun nanofiber as building blocks for a novel eco-friendly air filtration membrane: A review.* Separation and Purification Technology, 2021. **277**: p. 119623.
11. Mohana, A.A., et al., *Nano/microplastics: Fragmentation, interaction with co-existing pollutants and their removal from wastewater using membrane processes.* Chemosphere, 2022. **309**: p. 136682.
12. Adepu, S. and S. Ramakrishna, *Controlled drug delivery systems: current status and future directions.* Molecules, 2021. **26**(19): p. 5905.
13. Ahuja, G. and K. Pathak, *Porous carriers for controlled/modulated drug delivery.* Indian journal of pharmaceutical sciences, 2009. **71**(6): p. 599.
14. Jantzen, G.M. and J.R. Robinson, *Sustained-and controlled-release drug delivery systems.* Drugs and The Pharmaceutical Sciences, 2002. **121**: p. 501-528.
15. Kashkooli, F.M., M. Soltani, and M. Souri, *Controlled anti-cancer drug release through advanced nano-drug delivery systems: Static and dynamic targeting strategies.* Journal of controlled release, 2020. **327**: p. 316-349.
16. Sun, T., et al., *Development of a 3D cell culture system for investigating cell interactions with electrospun fibers.* Biotechnology and bioengineering, 2007. **97**(5): p. 1318-1328.
17. Neumann, T., S.D. Hauschka, and J.E. Sanders, *Tissue engineering of skeletal muscle using polymer fiber arrays.* Tissue engineering, 2003. **9**(5): p. 995-1003.
18. Cheng, Q., et al., *Engineering the microstructure of electrospun fibrous scaffolds by microtopography.* Biomacromolecules, 2013. **14**(5): p. 1349-1360.
19. Pensabene, V., et al. *Optimization of electrospun fibrous membranes for in vitro modeling of blood-brain barrier*. in *2016 38th Annual International Conference of the IEEE Engineering in Medicine and Biology Society (EMBC)*. 2016. IEEE.

20. Wang, Z., et al., *Dual-microstructured porous, anisotropic film for biomimicking of endothelial basement membrane.* ACS applied materials & interfaces, 2015. **7**(24): p. 13445-13456.
21. Casillo, S.M., et al., *Membrane pore spacing can modulate endothelial cell–substrate and cell–cell interactions.* ACS biomaterials science & engineering, 2017. **3**(3): p. 243-248.
22. Murphy, C.M., M.G. Haugh, and F.J. O'brien, *The effect of mean pore size on cell attachment, proliferation and migration in collagen–glycosaminoglycan scaffolds for bone tissue engineering.* Biomaterials, 2010. **31**(3): p. 461-466.
23. Chung, H.H., et al., *Use of porous membranes in tissue barrier and co-culture models.* Lab on a Chip, 2018. **18**(12): p. 1671-1689.
24. Quirós-Solano, W., et al., *Microfabricated tuneable and transferable porous PDMS membranes for Organs-on-Chips.* Scientific reports, 2018. **8**(1): p. 13524.
25. Kim, M.Y., et al., *Microfabrication of high-resolution porous membranes for cell culture.* Journal of membrane science, 2014. **452**: p. 460-469.
26. Huh, D., et al., *Microfabrication of human organs-on-chips.* Nature protocols, 2013. **8**(11): p. 2135-2157.
27. Baji, A., et al., *Electrospinning of polymer nanofibers: Effects on oriented morphology, structures and tensile properties.* Composites science and technology, 2010. **70**(5): p. 703-718.
28. Xie, J., et al., *Electrospun nanofibers for neural tissue engineering.* Nanoscale, 2010. **2**(1): p. 35-44.
29. Wang, R., et al., *Electrospun nanofibrous membranes for high flux microfiltration.* Journal of Membrane Science, 2012. **392**: p. 167-174.
30. Sun, D., et al., *Near-field electrospinning.* Nano letters, 2006. **6**(4): p. 839-842.
31. Shin, D., J. Kim, and J. Chang, *Experimental study on jet impact speed in near-field electrospinning for precise patterning of nanofiber.* Journal of Manufacturing Processes, 2018. **36**: p. 231-237.
32. Nazemi, M.M., A. Khodabandeh, and A. Hadjizadeh, *Near-field electrospinning: crucial parameters, challenges, and applications.* ACS Applied Bio Materials, 2022. **5**(2): p. 394-412.
33. Yan, F., et al., *A multi-scale controlled tissue engineering scaffold prepared by 3D printing and NFES technology.* AIP Advances, 2014. **4**(3).
34. Kolan, K.C., et al., *Near-field electrospinning of a polymer/bioactive glass composite to fabricate 3D biomimetic structures.* International Journal of Bioprinting, 2019. **5**(1).
35. Tsai, L., et al. *Study of the drug fiber for wound healing by direct-writing near field electrospinning with subdivision control*. in *2017 International Conference on Applied System Innovation (ICASI)*. 2017. IEEE.
36. Mai, Z., et al., *PCL/collagen/UA composite biomedical dressing with ordered microfiberous structure fabricated by a 3D near-field electrospinning process.* Polymers, 2022. **15**(1): p. 223.
37. Hsieh, S.T., et al., *Near-field electrospinning of polymer/phage whispering gallery mode microfiber resonators for label-free biosensing.* Sensors and Actuators B: Chemical, 2022. **367**: p. 132062.
38. Fuh, Y.-K. and H.-S. Hsu, *Fabrication of monolithic polymer nanofluidic channels via near-field electrospun nanofibers as sacrificial templates.* Journal of Micro/Nanolithography, MEMS and MOEMS, 2011. **10**(4): p. 043004-043004-5.
39. Mikos, A.G., et al., *Preparation of poly (glycolic acid) bonded fiber structures for cell attachment and transplantation.* Journal of biomedical materials research, 1993. **27**(2): p. 183-189.
40. Li, L., R. Hashaikeh, and H.A. Arafat, *Development of eco-efficient micro-porous membranes via electrospinning and annealing of poly (lactic acid).* Journal of membrane science, 2013. **436**: p. 57-67.
41. Lombard, J.D.S., et al., *Thermal treatment of electrospun polystyrene fibers: microstructural evolution and mechanical behavior.* Journal of Materials Science, 2023. **58**(13): p. 6009-6024.

42. Fan, P.W., et al., *Annealing effect on electrospun polymer fibers and their transformation into polymer microspheres.* Macromolecular rapid communications, 2012. **33**(4): p. 343-349.
43. Meng, Z., et al., *Electrospinning of PLGA/gelatin randomly-oriented and aligned nanofibers as potential scaffold in tissue engineering.* Materials Science and Engineering: C, 2010. **30**(8): p. 1204-1210.
44. Sadeghi, A., et al., *Surface modification of electrospun PLGA scaffold with collagen for bioengineered skin substitutes.* Materials science and engineering: C, 2016. **66**: p. 130-137.
45. Shin, H.J., et al., *Electrospun PLGA nanofiber scaffolds for articular cartilage reconstruction: mechanical stability, degradation and cellular responses under mechanical stimulation in vitro.* Journal of Biomaterials Science, Polymer Edition, 2006. **17**(1-2): p. 103-119.
46. Pan, Z. and J. Ding, *Poly (lactide-co-glycolide) porous scaffolds for tissue engineering and regenerative medicine.* Interface focus, 2012. **2**(3): p. 366-377.
47. Liu, X., et al., *Electrospinnability of poly lactic-co-glycolic acid (PLGA): the role of solvent type and solvent composition.* Pharmaceutical research, 2017. **34**: p. 738-749.
48. Zhao, W., et al., *Fabrication of functional PLGA-based electrospun scaffolds and their applications in biomedical engineering.* Materials Science and Engineering: C, 2016. **59**: p. 1181-1194.

Supplementary Information

Fabrication and customization of highly porous PLGA membranes utilizing near-field electrospinning, thermal transitions, and multilayer strategies

Noori Na, Minju Kim, Jungkyu Kim*, and Jiyoung Chang*

Department of Mechanical Engineering, University of Utah, Salt Lake City, USA

Corresponding author: jy.chang@utah.edu, jkim@mech.utah.edu

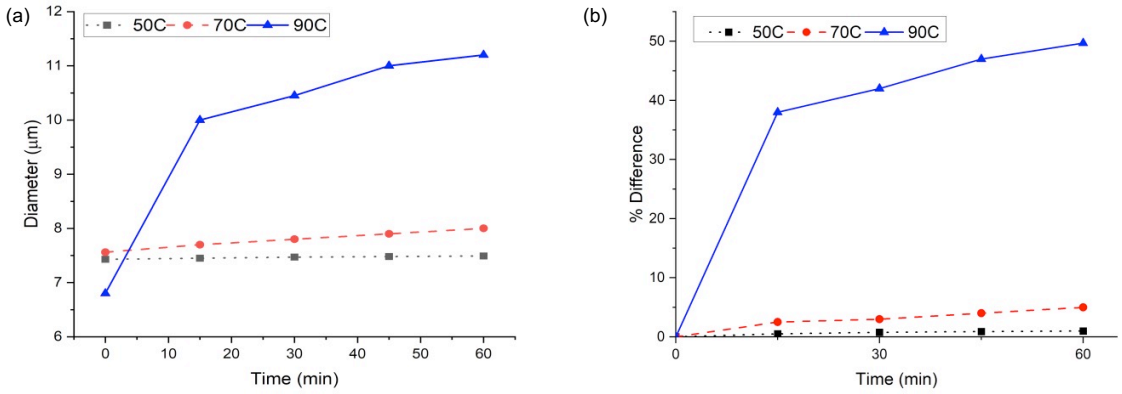

Figure S1. (a) Average PLGA fiber diameter changes in 50°C, 70°C, 90°C overtime (b) Diameter difference in different temperatures overtime

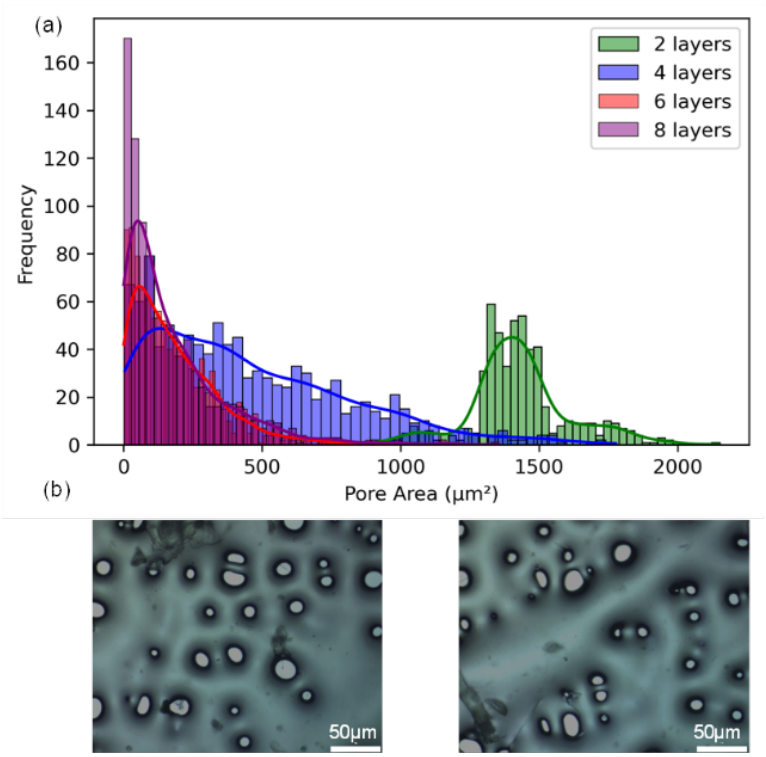

Figure S2. (a) Pore size distributions for 2,4,6,8 layer counts, demonstrating pore size modulation of different layers (b) After 1 hour heat treatment 8 layers of membrane